AD-A048 266 ROCKWELL INTERNATIONAL THOUSAND OAKS CALIF SCIENCE --ETC F/G 19/1
IMPACT DAMAGE IN BRITTLE MATERIALS IN THE PLASTIC RESPONSE REGI--ETC(U)
UNCLASSIFIED SEP 77 A G EVANS, M E BULDEN, G E EGGUM N00014-75-C-0669
SC5023.10TR NL

1 OF 1
AD A048266

END
DATE FILMED
1 -78
DDC

(12)

SC5023.10TR

COPY NO. 16

IMPACT DAMAGE IN BRITTLE MATERIALS IN THE ELASTIC RESPONSE REGIME

Technical Report

1st Jan. 1977 thru 30 Sept. 1977

Contract No. N00014-75-C-0669

Project No. 471

Submitted to:

Office of Naval Research
800 N. Quincy Street
Arlington, VA 22217

This Research was Sponsored by the Office of Naval Research
Under Contract No. N00014-75-C-0669 (Project No. 471)

Science Center
Rockwell International

Unclassified

SECURITY CLASSIFICATION OF THIS PAGE (When Data Entered)

REPORT DOCUMENTATION PAGE

READ INSTRUCTIONS BEFORE COMPLETING FORM

1. REPORT NUMBER

2. GOVT ACCESSION NO.

3. RECIPIENT'S CATALOG NUMBER

4. TITLE (and Subtitle)
(6) IMPACT DAMAGE IN BRITTLE MATERIALS IN THE PLASTIC RESPONSE ~~REGIME~~ Regime.

(9) 5. TYPE OF REPORT & PERIOD COVERED
Technical rept. 1 Jan-30 Sep 77,
Jan. 1, 1977 thru Sept. 30, 77

(14) 6. PERFORMING ORG. REPORT NUMBER
SC5023.10TR

7. AUTHOR(s)
(10) A. G./Evans, M. E./Bulden, G. E./Eggum M./Rosenblatt

(15) 8. CONTRACT OR GRANT NUMBER(s)
N0014-75-C-0669

9. PERFORMING ORGANIZATION NAME AND ADDRESS
Rockwell International
Science Center
Thousand Oaks, CA 91360

10. PROGRAM ELEMENT, PROJECT, TASK AREA & WORK UNIT NUMBERS
Project No. 471

11. CONTROLLING OFFICE NAME AND ADDRESS
Office of Naval Research
800 N. Quincy Street
Arlington, VA 22217 (Code 471)

12. REPORT DATE
Sept. 30, 1977 (11) 30 Sep 77

13. NUMBER OF PAGES
35

14. MONITORING AGENCY NAME & ADDRESS (if different from Controlling Office)

15. SECURITY CLASS. (of this report)
Unclassified (12) 41 p.

15a. DECLASSIFICATION/DOWNGRADING SCHEDULE

16. DISTRIBUTION STATEMENT (of this Report)

Reproduction in Whole or in Part is Permitted for any Purpose of the United States Government.

17. DISTRIBUTION STATEMENT (of the abstract entered in Block 20, if different from Report)

18. SUPPLEMENTARY NOTES

19. KEY WORDS (Continue on reverse side if necessary and identify by block number)
Impact, erosion, ceramics, projectiles, toughness, hardness

389 949

20. ABSTRACT (Continue on reverse side if necessary and identify by block number)
The impact damage created in the plastic response regime has been characterized in terms of the surface extension and the penetration of the fractures. A numerical dynamic analysis has been performed (of a typical impact within this regime) to indicate some of the principal characteristics of the contact behavior and the stress field. The damage has then been analyzed - using simplified postulates based on key features of the impact dynamics and the quasi-static indentation fracture - which has enabled the primary material and target parameters affecting the impact fracture to be identified. Thereafter, some implicaitons for strength

DD FORM 1 JAN 73 1473 EDITION OF 1 NOV 65 IS OBSOLETE

Unclassified

SECURITY CLASSIFICATION OF THIS PAGE (When Data Entered)

degradation and erosion have been discussed.

SC5023.10TR

ON IMPACT DAMAGE IN THE ELASTIC RESPONSE REGIME

By

A. G. Evans

Rockwell International Science Center

Thousand Oaks, California 91360

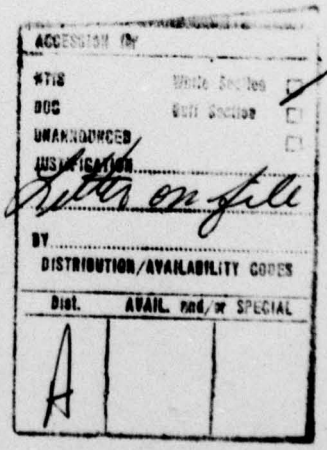

TABLE OF CONTENTS

ABSTRACT

The damage created by the impact of soft projectiles onto a brittle target has been examined. The character of the damage near the threshold has been evaluated, and damage parameters that indicate the important target properties affecting the incidence of damage have been derived. The fracture toughness and elastic wave velocity have been identified as target variables of primary importance, and their significance has been verified experimentally.

1.0 INTRODUCTION

The character of the damage created by the impact of a projectile onto a brittle material depends on the target response, elastic or plastic[1] (this response is determined, in turn, by the relative plastic deformation properties, acoustic impedence, etc., of the projectile and the target). The damage that occurs in the plastic response regime is now reasonably well understood and has been characterized[2] primarily in terms of the toughness K_C and macrohardness H of the target. However, the damage in the elastic response regime is still poorly comprehended. The initial damage in this regime is found to occur as short, circumferential surface cracks (Fig. 1). These cracks have been attributed to the activation of small pre-existing cracks by the relatively large tangential tensile stresses associated with the Rayleigh wave.[1,3,4] An approximate analytic solution for the spatial and temporal features of the tensile stress pulse has indicated that the threshold should be influenced by the following target properties:[1] the size distribution of pre-existing surface cracks, the fracture toughness, and the elastic wave velocity. However, the relative importance and the magnitude of the effects attributed to each of these variables has not been established. The present paper generates information pertinent to this problem.

The problem is addressed by examining the variables that influence both the dynamic elastic stresses and the crack propagation characteristics under stress wave loading. The interrelationships between these variables are then used to identify impact damage parameters. Finally, the utility of the damage parameters is explored experimentally.

2.0 IMPACT STRESSES

There are a limited number of solutions for the dynamic elastic stresses, σ, generated by the impact of compressive projectiles.[5,6] These stresses are dictated essentially by the impact pressure, p(t), the contact radius between the projectile and target, b(t), and the deflection of the target surface. The only detailed stress analyses have been performed for rigid surfaces; a condition that affords a reasonable approximation to a damage regime of considerable present concern--soft projectiles (such as water) impacting brittle ceramic (high modulus) surfaces. For this condition, numerical analyses[6] suggest the pressure distribution, prior to extensive lateral outflow, shown in Fig. 2 (at longer times, during lateral outflow, the pressure should, of course, gradually decline). An analytic solution for the dyanmic stresses that develop in response to this pressure has been obtained[5] by approximating the pressure distribution with a uniform pressure, expanding as the square root of time, t. The important features of the analysis are:

(i) its recognition of stress field normalization through the material independent parameters

$$\Omega = \sigma/p$$
$$T = 4v_\ell{}^2 t/k^2 \qquad (1)$$
$$R = 4v_\ell r/k^2$$

where r is the distance from the impact center, v_ℓ is the longitudinal wave velocity, and k is a projectile dependent parameter, determined primarily by the

projectile radius r_p and its initial velocity v_o ($k^2 \sim 2r_p v_o$).

(ii) the occurrence of a maximum in the peak tensile stress $\hat{\sigma}(r)$ close to the impact center (Fig. 3).

(iii) the steep tensile stress gradient from the surface to the interior (Fig. 4).

Numerical stress analyses (derived by applying the pressure distribution of Fig. 2 to an elastic half space) have confirmed the existence of a maximum in $\hat{\sigma}(r)$ adjacent to the impact center.[6] The analyses have not been extended to the post-outflow stress development, but it is reasonable to anticipate that the stress will decline at a more rapid rate than in the pre-outflow regime. Since outflow is essentially independent of the target (it is determined primarily by the wave propagation and deformation properties of the projectile), the stress decay will be manifested closer to the impact center for those materials with higher wave velocities. A schematic of the temporal and spatial features of the near surface radial tensile stress (that incorporates the principal effects noted above) is plotted in Fig. 3, for materials with two different wave velocities, $v_{\ell_1} \approx v_{\ell_2}$. Note that the duration and spatial extent of the stress pulse are substantially smaller for the material with the higher wave velocity. It has been assumed that lateral outflow occurs well beyond the maximum in $\hat{\sigma}$ so that the stress levels of primary concern for fracture ($\Omega > \Omega_c$) are unaffected by the outflow process. When this assumption becomes invalid (perhaps in materials with low wave velocities, e.g., polymers), the outflow process could dimish in the prospective fracture zone, thereby retarding damage formation. Another important feature of the stress field is the gradient in the

radial tensile stress beneath the surface. This is exemplified in Fig. 4, wherein the stress gradient is examined for the same two velocities ($v_{\ell_1} = 2v_{\ell_2}$) at equivalent locations (e.g., at the positions, r_1 and r_2, where the peak tensile stress exhibits its maximum value, $\hat{\sigma}_m$). This gradient should be directly proportional to the wave velocity.

3.0 DYNAMIC CRACK PROPAGATION

Crack activation and growth in dynamic stress fields is determined by both the temporal and spatial details of the stress at the crack surface. A generalized theory that allows both the temporal and spatial effects to be treated simultaneously has not yet been developed. However, an appreciation for these effects can be constructed by examining them on a separate basis.

3.1 Temporal Effects

The problem of a spatially uniform stress pulse impinging onto a crack has been explored in several recent studies.[7,8] The following sequence of events appears to prevail. When the stress wave first impinges on the crack, the wave is diffracted by the crack surface, and the stress σ_L ahead of the crack increases with time, t. An analytical expression for the stress, derived from Freund,[7] is:

$$\sigma_L = \frac{\sigma_o}{\pi}\left[\frac{2}{(1-\nu^2)}\left(\frac{t}{r}\right) v_\ell\right]^{1/2} \qquad (2)$$

where σ_o is the amplitude of the stress, r is the distance from the crack tip, v_ℓ is the longitudinal wave velocity* and ν is Poisson's ratio. The equivalent stress intensity factor, K, is

---

*For a surface crack, it has been pointed out by M. V. Swain (private communication) that the Rayleigh velocity, v_r, might be the appropriate velocity term in Eq. (2).

$$K = 2\sigma_o \left[\frac{v_\ell t}{\pi(1-\nu^2)} \right]^{1/2} \qquad (3)$$

The stress intensity factor thus exhibits a square root dependence on time and its magnitude is <u>independent</u> of the crack length. Hence, if K reaches the critical value K_c while Eq. (3) still pertains, the incubation time τ for crack activation becomes

$$\tau = \frac{\pi}{4} \frac{K_c^2 (1-\nu^2)}{v_\ell \sigma_o^2} \qquad (4)$$

An analogous expression (referred to as a "least action law") has been obtained by Steverding and Lehnigk,[9] using a thermodynamic analysis. However, Eq. (4) only pertains until the stresses are perturbed by the wave diffracted at the opposite crack tip (or the wave reflected at the surface for a surface crack). This occurs when $t \approx 2a/v_\ell$, where 2a is the crack length.[8] The post-collision wave pattern is distorted and K increases less rapidly with time than anticipated by Eq. (2). Solutions for K(t) have been derived by Sih and colleagues.[8] These solutions can be expressed in the form

$$K(t) = f\left(\frac{v_\ell t}{a}\right) K_s \qquad (5)$$

where K_s is the quasistatic stress intensity factor and f are the functions plotted in Fig. 5. The principal feature to note is that K reaches a peak value $\hat{K}$ that exceeds the quasi static stress intensity factor (by a factor ~1.2), and then oscillates about the static value as a damped sinusoid. A more general expression for the incubation time can now be derived from Eq. (5), as

$$\frac{v_\ell \tau}{a^*} = g\left(\frac{a}{a^*}\right) \tag{6}$$

where a* is a parameter defined by;

$$a^* = \frac{1}{\pi}\left(\frac{K_c}{\sigma_o}\right)^2 \tag{7}$$

and g is the function plotted for a through crack in Fig. 6. A zone of "no fracture" is evident. This zone is bounded by a critical crack size minimum $a_c \approx 0.63\ a^*$ (dictated by the condition that the peak stress intensity factor $\hat{K} < K_c$), and by the incubation time. The existence of fracture thresholds of this type has recently been demonstrated by Kalthoff and Shockey.[10] This incubation bound is identical to that for the semi-infinite crack, except for cracks very close to the critical size ($1.0 > a/a_c \leq 0.8$) - even then the divergence is small. It seems plausible, therefore, that the subsequent motion of a through crack (after incubation) should be reasonably well described by solutions derived for semi-infinite cracks. The most comprehensive solution, due to Freund,[7,11] can be expressed in the form

$$\dot{a}/v_r = 1 - \frac{K_c^2 (1 - \nu^2)}{2\sigma_o^2 v_\ell [t^{1/2} - (t - t_o)^{1/2} H(t - t_o)]^2} \tag{8}$$

where t_o is the pulse duration and H is the unit step function. This expression predicts that once the incubation time has been exceeded ($t > \tau$), the crack accelerates according to

$$\dot{a}/v_r \approx 1 - \pi K_c^2 / 4\sigma_o^2 v_\ell t \tag{9}$$

while, after the pulse has passed the crack plane ($t > t_o$), the crack accelerates

$$\dot{a}/v_r \approx 1 - \pi K_c^2 / 4\sigma_o^2 v_\ell [t^{1/2} - (t - t_o)^{1/2}]^2 \tag{10}$$

and finally arrests, as illustrated in Fig. 7. The crack increment Δa above the threshold (Appendix) is;

$$\frac{\Delta a}{v_r t} = \frac{1}{4}\left[6\frac{t_o}{\tau} + \frac{t_o^2}{\tau^2} - 3\right] - \ell n\left(\frac{t_o}{\tau}\right) - \frac{1}{4}\left[\frac{2\sqrt{1 + 4t_o\tau/(\tau + t_o)^2}}{\left(\sqrt{1 + 4t_o\tau/(\tau + t_o)^2} - 1\right)} - \ell n \left(\frac{\sqrt{1 + 4t_o\tau/(\tau + t_o)^2} + 1}{\sqrt{1 + 4t_o\tau/(\tau + t_o)^2} - 1}\right)\right]$$

The motion of an embedded penny crack or a surface half-penny crack may be numerically different from that predicted by Eq. (8), as might be anticipated from the differing time dependencies of K for static cracks (Fig. 5). However, the relative dependencies on the important material variables should be essentially the same.

3.2 Spatial Effects

When a crack is subjected to a spatially varying tensile stress, the crack propagation condition can exhibit several unique characteristics. These special features can be deduced by estimating the stress intensity factors for cracks penetrating steep stress gradients. If the crack is relatively small compared to the sample dimension, W (i.e., $a/W \lesssim 0.2$), the stress intensity factor for a through-thickness surface crack of depth a in a spatially varying stress, $\sigma(z)$ is given by;[12]

$$K = 2\sqrt{\frac{a}{\pi}} \int_0^a \frac{\sigma(z)\,[1 + F(z/a)]\,dz}{\sqrt{a^2 - z^2}} \qquad (11)$$

where F(z/a) is given by;

$$F(z/a) = [1 - z/a]\,[0.295 - 0.391\ (z/a)^2 + 0.769\ (z/a)^4 - 0.994\ (z/a)^6 + 0.509\ (z/a)^8]$$

A functional form for $\sigma(z)$ that allows the important stress gradient phenomena to be conveniently illustrated (Fig. 8) is the exponential form;

$$\sigma(z) = \sigma_o e^{-z/z_o} \tag{12}$$

where z_o is a constant that provides a measure of the severity of the gradient and σ_o is the peak (surface) amplitude. Substituting Eq. (12) into Eq. (11) and rearranging gives;

$$\frac{K}{\sqrt{z_o}} = 2\sigma_o \sqrt{\frac{1}{\pi}\left(\frac{a}{z_o}\right)} \int_0^{a/z_o} \frac{e^{-z/z_o}\left[1 + F\left(a/z_o,\ z/z_o\right)\right] d(a/z_o)}{\sqrt{(a/z_o)^2 - (z/z_o)^2}}$$

$$\equiv 2\sigma_o \sqrt{\frac{1}{\pi}\left(\frac{a}{z_o}\right)} \left[I\ (a/z_o)\right] \tag{13}$$

Setting K equal to the critical value K_c allows the critical peak stress for crack propagation, σ_{oc}, to be expressed as;

$$\frac{\sigma_{oc}\sqrt{z_o}}{K_c} = \frac{1}{2I(a/z_o)} \sqrt{\frac{\pi}{(a/z_o)}} \tag{14}$$

4.0 DAMAGE PARAMETERS

Damage parameters--that classify the respective roles of the important material properties on the impact damage--can be generated by combining the information developed in the preceding sections concerning impact stress wave characteristics and dynamic fracture phenomena. (For this purpose, the shape of the tensile stress pulse is considered to exert a minor influence on the relative roles of the important material parameters, and the solutions for the step profile are used directly.)

Firstly, the incubation time (Eq. (4)) can be combined with the pulse duration and amplitude (Eq. 1)) to demonstrate the existence of a threshold contact pressure p_{c1} for the crack activation. This threshold is a lower bound, that pertains to cracks larger than a "critical" size a_c, and is given by;

$$p_{c1}^2 = \left[\frac{\pi}{\Omega_o^2 T_o}\right] \frac{\left(K_c^2 v_\ell\right)}{k^2} \tag{15}$$

where T_o and Ω_o are the material independent pulse duration and pulse amplitude, respectively, at the location where the <u>product</u> of the pulse duration and the square of the amplitude is a maximum (Fig. 3). If damage parameters D are now defined, in the sense that <u>enhanced</u> damage resistance is imparted by <u>increasing</u> D, then the target damage parameter for the incubation threshold, D_{T1}, is;

$$D_{T1} = K_c^2 v_\ell \tag{16}$$

This result is plotted in Fig. 8. It is apparent that for $a \lesssim z_o$ the crack can grow unstably, by an amount $\delta a^{\dagger}$ (that can substantially exceed the initial size, a_o, Fig. 8); whereas, for $a \gtrsim z_o$ crack growth is stable and only occurs while the stress continues to increase. It is also evident that there is an <u>absolute</u> fractor threshold σ_{th}, below which no crack extension can occur <u>regardless</u> of crack size, given by; $\sigma_{th} \approx K_c/\sqrt{z_o}$. Finally, it is important to note the relatively large flaw size range, $3 \times 10^{-1} \lesssim a/z_o \lesssim 3$, for which the activation stress σ_{oc} is flaw size insensitive. The details of the crack growth behavior under stress wave loading will be different, but similar trends with relative crack depth should exist. One important difference between static and dynamic crack activation derives from the larger dynamic value of K. This causes $\sigma_{oc}\sqrt{z_o}/K_c$ for a through crack to be reduced by ~ 0.25, as shown in Fig. 8.

---

† When the crack length is small relative to the sample dimensions, crack arrest occurs at $K \approx K_c$.[13]

while the projectile damage parameter D_{p1} is

$$D_{p1} = K^{-2} \approx r_p^{-1} v_o^{-1} \tag{17}$$

(The Hugoniot of the projectile is also important, of course, because of its influence on the interdependence of the pressure and projectile velocity.)

An additional threshold effect, independent of the crack size, derives from the stress gradient (Eq. (14)). Combining this result with the stress field normalization (Eq. (1)) gives;

$$P^2_{c2} = \left[\frac{4}{\hat{\Omega}^2 Z_o}\right] \frac{(K_c^2 v_\ell)}{k^2} \tag{18}$$

where Z_o and $\hat{\Omega}$ are the material independent stress gradient and amplitude, at the location where the surface pulse amplitude is a maximum (Fig. 4). The damage parameter for the stress gradient threshold is thus identical to that for the incubation threshold (Eq. (16)).

An apparent threshold might also derive from the crack extension behavior, because cracks are only observed, e.g., using optical or scanning electron microscopy, when they exceed a minimum size, a_m (determined by the residual crack opening displacement). Presuming that this minimum size is substantially in excess of the initial size a_o, the reduced crack extension result (Eq. (A10)) can be combined with Eq. (1) to yield

$$P^2_{C3} \approx \left[\frac{32\pi a_m}{T_o^2 \Omega_o^2}\right] \frac{\left(K_c^2 v_\ell^2\right)}{k^4} \tag{19}$$

The target damage parameter is thus

$$D_{T2} = K_c^2 v_\ell^2 \tag{20}$$

indicating a stronger dependence on the wave velocity than predicted by the other threshold conditions.

The size of the pre-existing cracks may also, of course, be important. Specifically, if these cracks were very small ($< 0.1 z_o$, see Fig. 8), the threshold p_{c2} would be substantially larger than predicted by Eq. (18). The role of the initial crack size can only be fully developed, however, when the details of the impact stress field have been elucidated (e.g., using numerical techniques). Hence, the damage parameter involving the initial crack size cannot yet be defined, except to recognize the existence of possible crack size effects when the cracks are small.

The growth of the damage above the threshold is less readily described by damage parameters. Initially, it involves the continued extension of cracks activated by prior impacts; this process can again be approximately described in Eq. (19). However, the subsequent crack growth and material removal process are much more complex, and a description of these processes is beyond our present capabilities.

5.0 IMPACT EXPERIMENTS

5.1 Experimental Techniques

Experiments have been designed to obtain a preliminary assessment of the utility of the target damage parameters D_{T1} and D_{T2} for describing the resistance of polycrystalline ceramics to impact damage (in the elastic response regime). For this purpose, precrack arrays (Fig. 9) have been introduced into samples of three polycrystalline materials, MgO, ZnS, and Si_3N_4 (Table 1), and the samples impacted near the centers of the crack arrays using 1 mm diameter nylon spheres. The crack arrays were introduced by Knoop indenters,[14] and the plastic zone subsequently removed by grinding and polishing. The indentation conditions were preselected,[15] to allow the crack sizes in each material to be approximately constant (~200 μm radius). This avoided ambiguities associated with possible crack size effects. The impact experiments were performed using an exploding foil technique;[16] a system which has the directional precision required for this series of experiments. The specific materials were chosen to enable the effects of K_c and γ_ℓ to be examined independently (Table 1).

5.2 Critical Velocities: Observation and Evaluation

Critical projectile velocities, v_c, were determined for each material by gradually increasing the velocity until crack activation was detected. An example of crack activation above the threshold is shown in Fig. 9 for the MgO material. The critical velocities obtained in this manner, for each of the three materials, are summarized in Table 1. It

is evident that the threshold velocity increases as both the wave velocity and the toughness increase, in qualitative accord with the damage parameters.

A more detailed comparison between theory and experiment can be affected by taking the contrast pressure p to be directly proportional to the projectile velocity (although this is not strictly correct, because of the nonlinear projectile response, the deviation should not be large in the velocity regime of present interest). Then, eqs. (15) or (18) predict the proportionality $v_c \propto K_c^{2/3} v_\ell^{1/3}$; while Eq. (19) predicts $v_c \propto K_c^{1/2} v_\ell^{1/2}$. A comparison of the critical velocities for MgO and Si_3N_4 indicate a toughness dependence of $\sim K^{2/3}$, consistent with the expectations of the damage parameters. However, a comparison for MgO and ZnS indicates a wave velocity dependence, $\sim v_\ell$, that is substantially larger than anticipated by the damage parameters. This discrepancy would reflect an additional effect of v_ℓ that has not yet been identified. Alternatively, the relatively coarse grain size of the ZnS (40 μm compared with ~ 2 μm for the MgO and Si_3N_4) could induce an effective near-surface crack propagation resistance* smaller than the indicated (polycrystalline) value, so that the comparison is not being effected at constant toughness. Further experimentation is needed to clarify this issue.

However, the results should not be reagrded as sufficiently definitive to assess the relative roles of D_{T1} and D_{T2}.

*The propagation of small cracks in relatively coarse grained materials is an ill-defined issue; but it is evident[13,17] that the crack must be at least 5-10 times the grain diameter before the crack propagation resistance assumes its polycrystalline value. For smaller crakcs, K_c varies between the single crystal and polycrystal values.

6.0 SUMMARY

The primary implications of both the theory and experiment are that the damage threshold in the elastic response regime is strongly influenced by both the wave velocity and toughness of the material. The wave velocity is a microstructure insensitive property, and its influence on the damage has implications primarily for the basic choice of the material, i.e., materials with a large modulus and low density such as Si_3N_4, SiC, Al_2O_3. By contrast, the toughness is highly microstructure sensitive,[19,20] and substantial opportunities exist for increasing the damage resistance by attending to the material's toughness. However, it is critical to recognize that the pertinent crack growth resistance relates to the extension of surface or near-surface cracks. This immediately establishes the importance of a fine surface grain size. The requirement for a fine scale microstructure essentially eliminates one important mode of toughening, controlled microfracture, which only pertains to relatively coarse grained ($\sim$ 10 μm) materials or to relatively coarse multiphase systems. Also, relatively tough two-phase metal/ceramic systems (e.g., WC/Co) may not be effective because of perturbations caused by deformation of the metal phase. Nevertheless, several attractive toughening approaches that can be applied to essentially single-phase systems, e.g., stress induced phase transformations, grain pull-out, seem pertinent.

The density of a material can be reduced by inducing porosity, but the effect is more than counteracted by the reduced modulus.[18]

The experiments conducted in this study are only regarded as preliminary. Further studies are needed to fully quantify the respective roles of the toughness and wave velocity (through the various damage paramters), especially on materials with microstructures of equilalent scale. The detailed influence of the pre-existing crack size also requires elucidation, particularly the possible enhancement of the damage resistance by developing materials with diminutive surface and near-surface pre-existing cracks.

REFERENCES

1. A. G. Evans and T. R. Wilshaw, Jnl. Mater. Sci., 12, 97 (1977)
2. A. G. Evans, M. E. Gulden, and M. Rosenblatt, "Impact Damage in the Plastic Response Regime," to be published
3. F. P. Bowden and J. E. Field, Proc. Roy. Soc., A282, 321 (1965)
4. W. F. Adler, Jnl. Mater. Sci., 12, 1253 (1977)
5. R. M. Blowers, Jnl. Inst. Maths. Applics., 5, 167 (1969)
6. M. Rosenblatt, unpublished results
7. L. B. Freund, Jnl. Mech., Phys. Solids, 21, 47 (1973)
8. G. C. Sih, "Handbook of Stress Intensity Factors," Lehigh University Press, p. 8.5.1-3 (1973)
9. B. Steverding, "Fracture Mechanics of Ceramics," (Ed. R. C. Bradt, D. P. Hasselman, and F. F. Lange), Plenum, New York, p. 287 (1976)
10. J. F. Kalthoff and D. Shockey, Jnl. Appl. Phys., 48, 986 (1977)
11. L. B. Freund, private communication
12. R. J. Hartranft and G. C. Sih, "Methods of Analysis and Solutions of Crack Problems," Ed., G. C. Sih, Noordhoff (1973)
13. A. G. Evans and T. G. Langdon, Prog. Mater. Sci., 21, 171 (1976)
14. J. J. Petrovic and M. G. Mendiratta, Jnl. Amer. Ceram. Soc., 59, 163 (1976)
15. A. G. Evans and E. A. Charles, Jnl. Amer. Ceram. Soc., 59, 403 (1976)

16. M. E. Graham, J. D. Carlyle, and T. L. Menna, Rev. Sci. Inst., 46, 1221 (1975)

17. R. W. Rice, "Fracture Mechanics of Ceramics," (Ed. R. C. Bradt, D. P. H. Hasselman, F. F. Lange), Plenum, New York, p. 323 (1974)

18. B. R. Tittmann, private conversation

19. A. G. Evans, A. H. Heuer, and D. Porter, Fourth International Fracture Conference, (Ed. D. M. R. Taplin), vol. 1, p. 529 (1977)

20. F. F. Lange, Conference of Fracture Mechanics of Ceramics, Penn State University, July 1977, in press

APPENDIX

The Crack Length Increment due to a Supercritical Stress Pulse

During the acceleration phase the crack velocity (Eqn.(8)) can be expressed in terms of the incubation time τ (eqn. 4) as;

$$\frac{da}{da} = v_r\,(1 - \tau/t) \tag{A1}$$

The crack increment, Δa, is thus simply;

$$\frac{\Delta a_1}{v_r} = \int_{\tau}^{t_o} (1 - \tau/t)\, dt \tag{A2}$$

$$= t_o - \tau - \tau \ell n(t_o/\tau)$$

In the deceleration phase, the crack velocity (Eqn. 8) is

$$\frac{da}{dt} = v_r \left[1 - \frac{\tau}{[t^{1/2} - (t-t_o)^{1/2}]^2}\right] \tag{A3}$$

The time t_a for the crack to arrest, after the pulse has passed, determined by setting the crack growth rate in Eqn. (A3) equal to zero, is thus;

$$\frac{t_a}{\tau} = \frac{(1 + t_{o/\tau})^2}{4} \tag{A4}$$

The crack increment Δa_2 is thus given by;

$$\frac{\Delta a_2}{v_r} = \int_{t_o}^{t_a + t_o} \left[1 - \frac{\tau}{[t^{1/2} - (t - t_o)^{1/2}]^2}\right] dt \qquad (A5)$$

To solve the integral, let

$$t = \frac{t_o}{1-x^2} \qquad (A6)$$

the integral becomes

$$\frac{\Delta a_2}{v_r} = t_a - 2\tau \int_o^{\beta} \frac{x dx}{(1-x^2)(1-x)^2} \qquad (A7)$$

where, $\beta = \sqrt{t_a/(t_o + t_a)}$. Integration then gives

$$\frac{\Delta a_2}{v_r} = t_a - \frac{\tau}{4}\left[\frac{2\beta}{(1-\beta)^2} - \ell n\left(\frac{1+\beta}{1-\beta}\right)\right] \qquad (A8)$$

The total crack length increment is thus,

$$\frac{\Delta a}{v_r \tau} = \frac{(t_a + t_o)}{\tau} - 1 - \ell n\left(\frac{t_o}{\tau}\right) - \frac{1}{4}\left[\frac{2\beta}{(1-\beta)^2} - 2\ell n\left(\frac{1+\beta}{1-\beta}\right)\right] \qquad (A9)$$

Note that for $t_o >> \tau$, Eqn. (A9) reduces to

$$\Delta a \approx \frac{V_r t_o^2}{8 \tau} \equiv \frac{V_r t_a}{2} \qquad \text{(A10)}$$

FIGURES

Figure 1 - Circumferential cracks produced by the impact of a nylon projectile on zinc sulphide.

Figure 2 - A numerical computation of the pressure profile produced by the impact of a water drop onto an elastic half space.

Figure 3 - A schematic of the spatial and temporal dependence of the tensile stress pulses produced by impact. The pulse shape and the stress envelope have been taken from calculations by Adler[4] and Rosenblatt.[6]

Figure 4 - A schematic of the stress profile at the position of peak surface stress amplitude.

Figure 5 - The time dependence of the stress intensity factor for through and penny cracks subjected to a step pulse.

Figure 6 - The fracture bounds derived from the dynamic crack activation analysis.

Figure 7 - A schematic indicating the motion of a crack subjected to a stress pulse.

Figure 8 - The conditions for the growth of a surface crack in an exponentially varying stress field.

Figure 9 - The activation of surface cracks in MgO by the impact of a 1 mm nylon sphere at 1100 ms^{-1}.

TABLE I

The Threshold Velocities for Pre-Cracked Materials
Impacted by 1mm Nylon Spheres

Material	Longitudinal Wave Speed (ms^{-1})	Toughness ($MPa\sqrt{m}$)	Average Grain Diameter (μm)	Threshold (ms^{-1}) Velocity
ZnS	4.6×10^3	1	40	400
MgO	9.4×10^3	1	2	800
Si_3N_4	10^4	5	1	2400

Figure 1

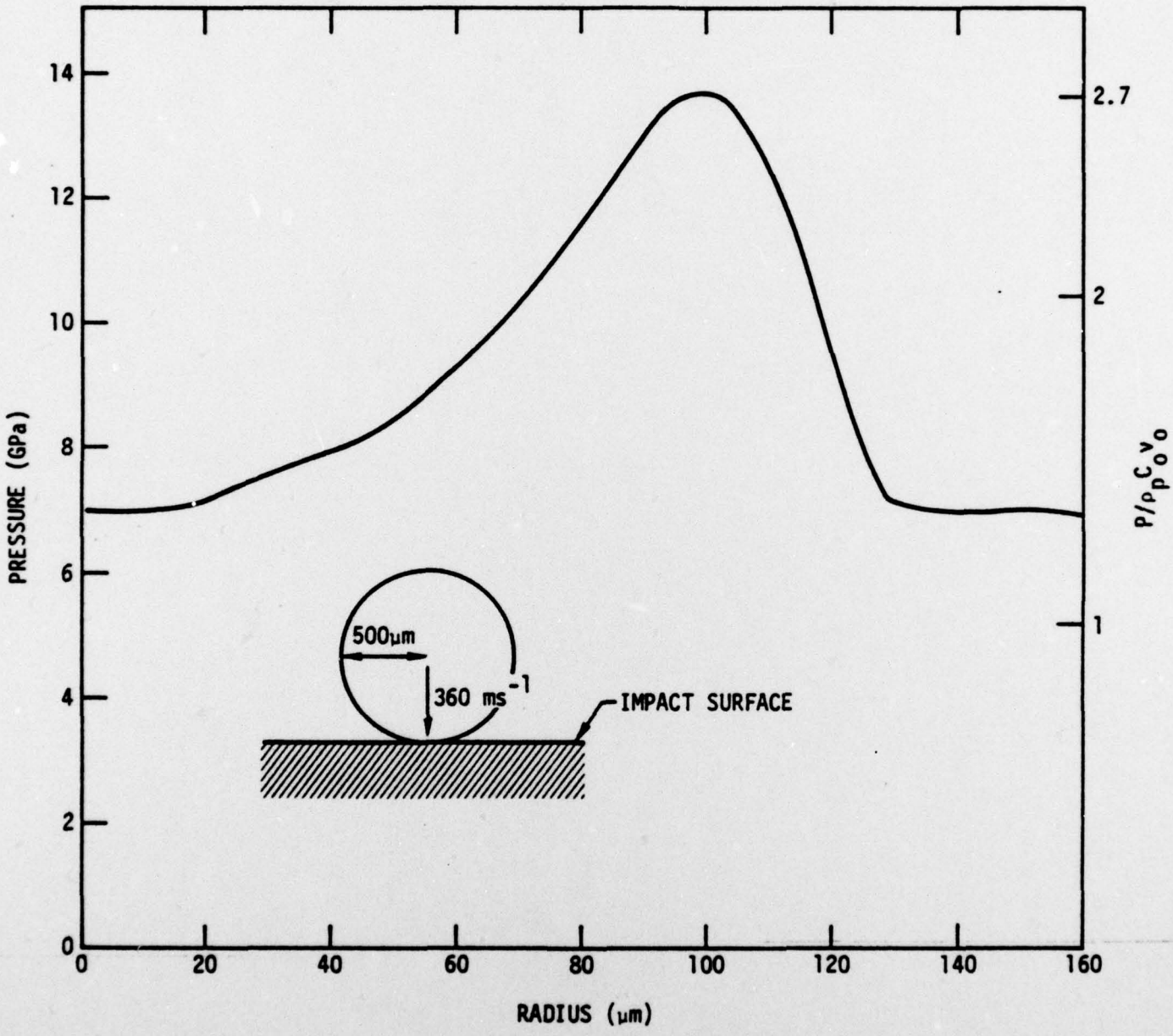
PRESSURE (GPa)
RADIUS (μm)
$P/\rho_p C_{p_o} v_o$
0
2
4
6
8
10
12
14
0
20
40
60
80
100
120
140
160
1
2
2.7
500μm
360 ms^{-1}
IMPACT SURFACE

Figure 2

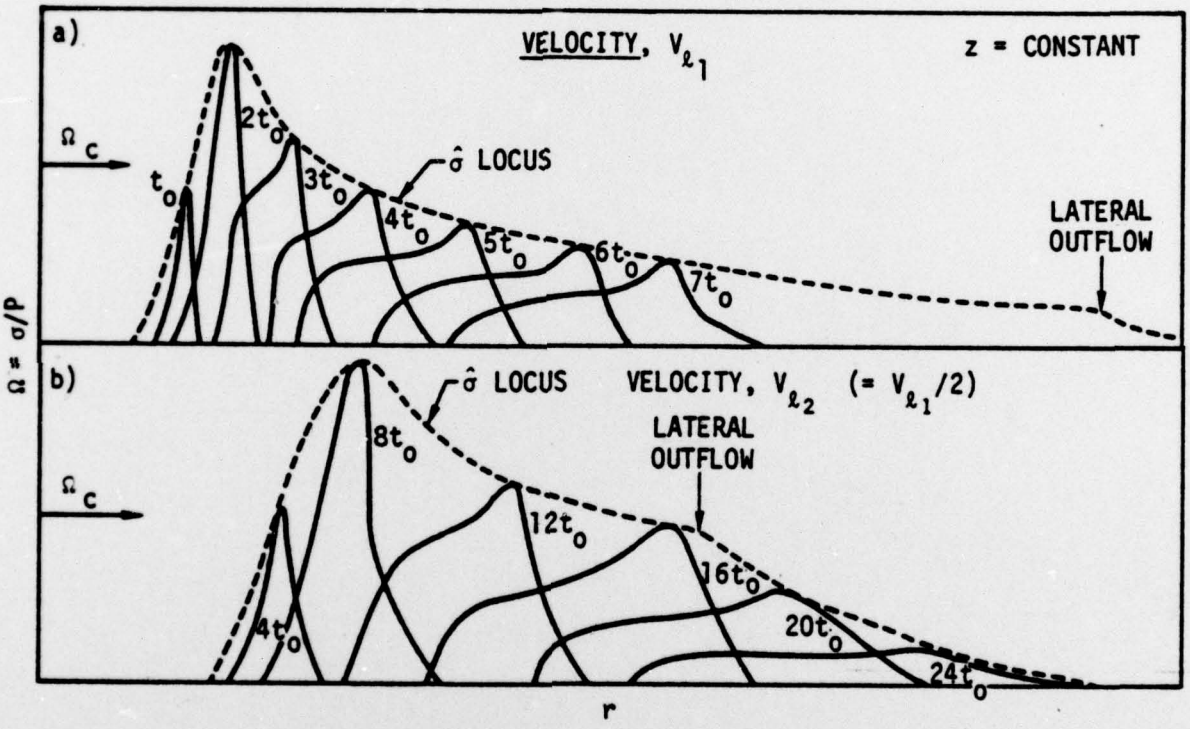
a)
VELOCITY, V_{ℓ_1}
z = CONSTANT
Ω_c
t_o
$2t_o$
$3t_o$
$\hat{\sigma}$ LOCUS
$4t_o$
$5t_o$
$6t_o$
$7t_o$
LATERAL OUTFLOW
b)
$\hat{\sigma}$ LOCUS
VELOCITY, V_{ℓ_2} (= $V_{\ell_1}/2$)
LATERAL OUTFLOW
$8t_o$
$12t_o$
$16t_o$
$20t_o$
$24t_o$
$4t_o$
$\Omega = \sigma/P$
r

Figure 3

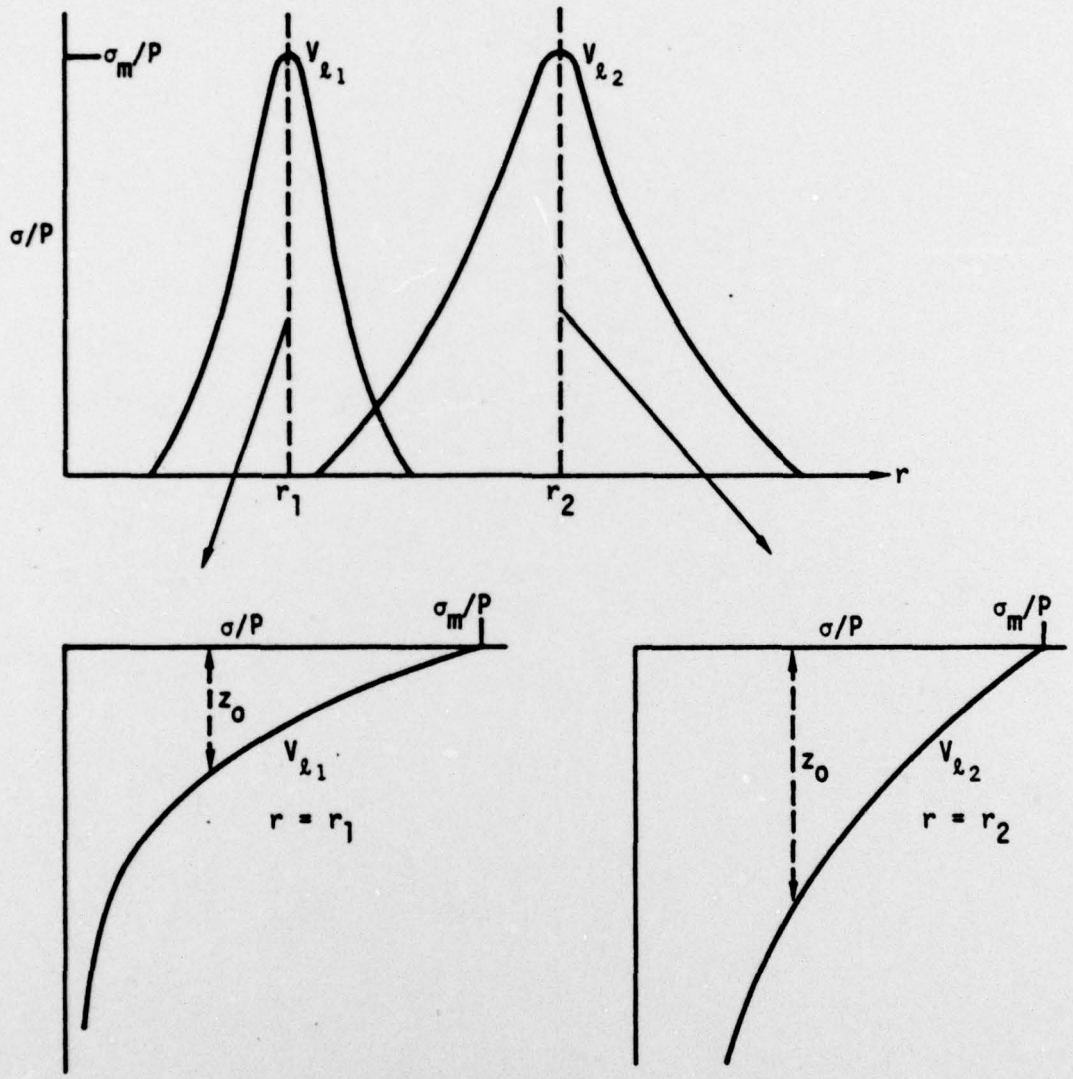

Figure 4

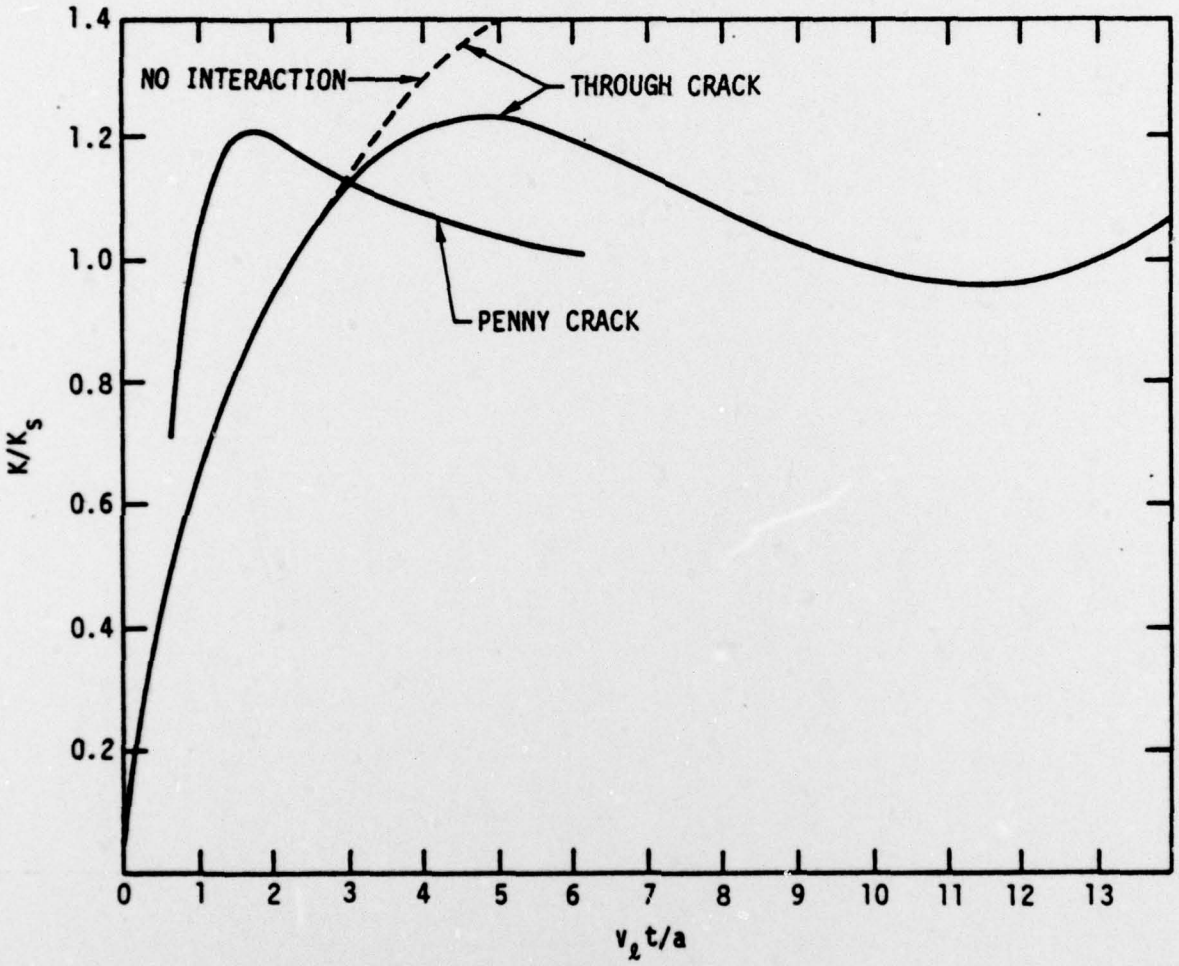
1.4
1.2
1.0
0.8
0.6
0.4
0.2
K/K_s
NO INTERACTION
THROUGH CRACK
PENNY CRACK
0
1
2
3
4
5
6
7
8
9
10
11
12
13
V_ℓ t/a

Figure 5

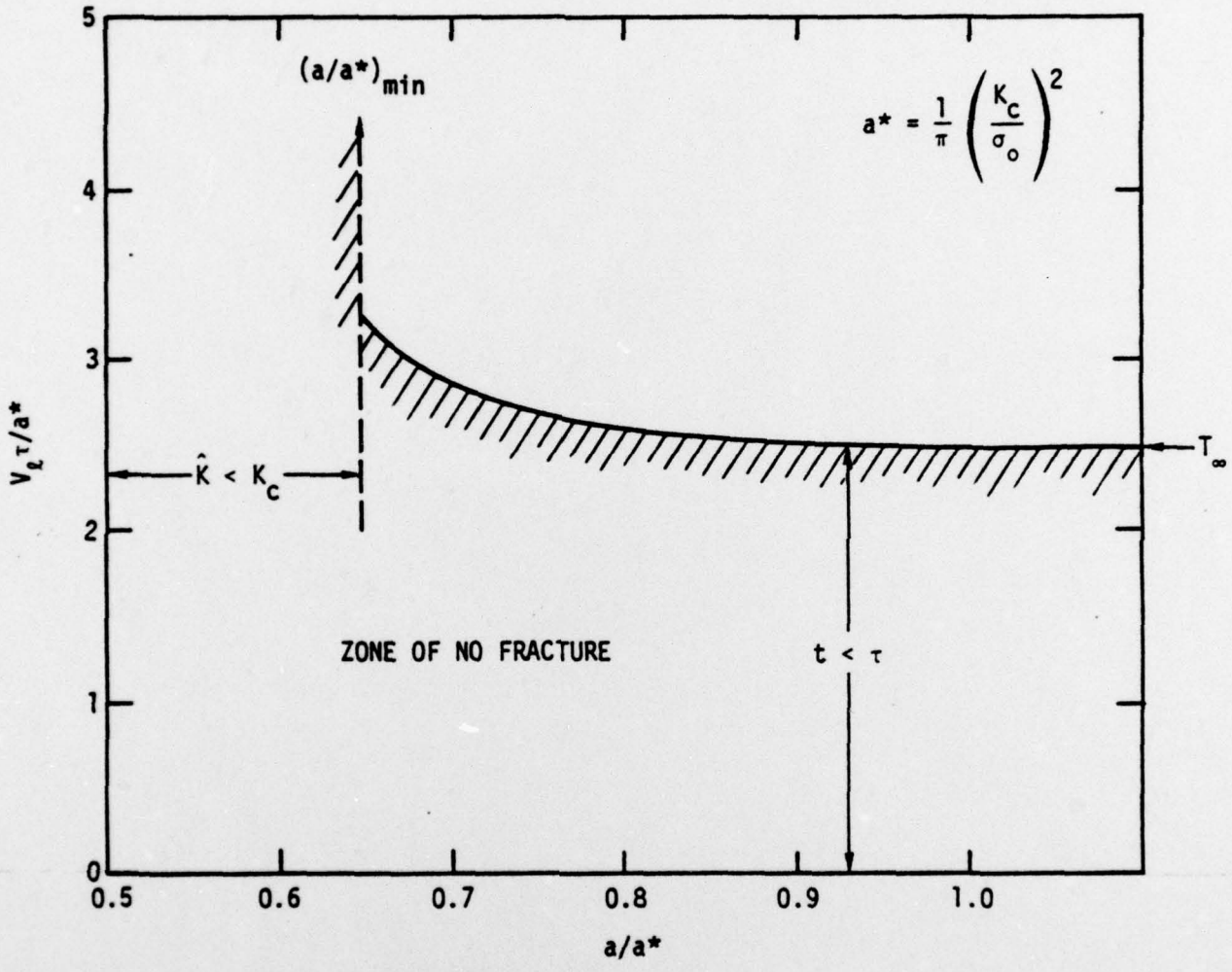
5
4
3
2
1
0
0.5
0.6
0.7
0.8
0.9
1.0
$(a/a^*)_{min}$
$a^* = \frac{1}{\pi}\left(\frac{K_c}{\sigma_o}\right)^2$
$V_\ell \tau/a^*$
$\hat{K} < K_c$
T_∞
ZONE OF NO FRACTURE
$t < \tau$
a/a^*

Figure 6

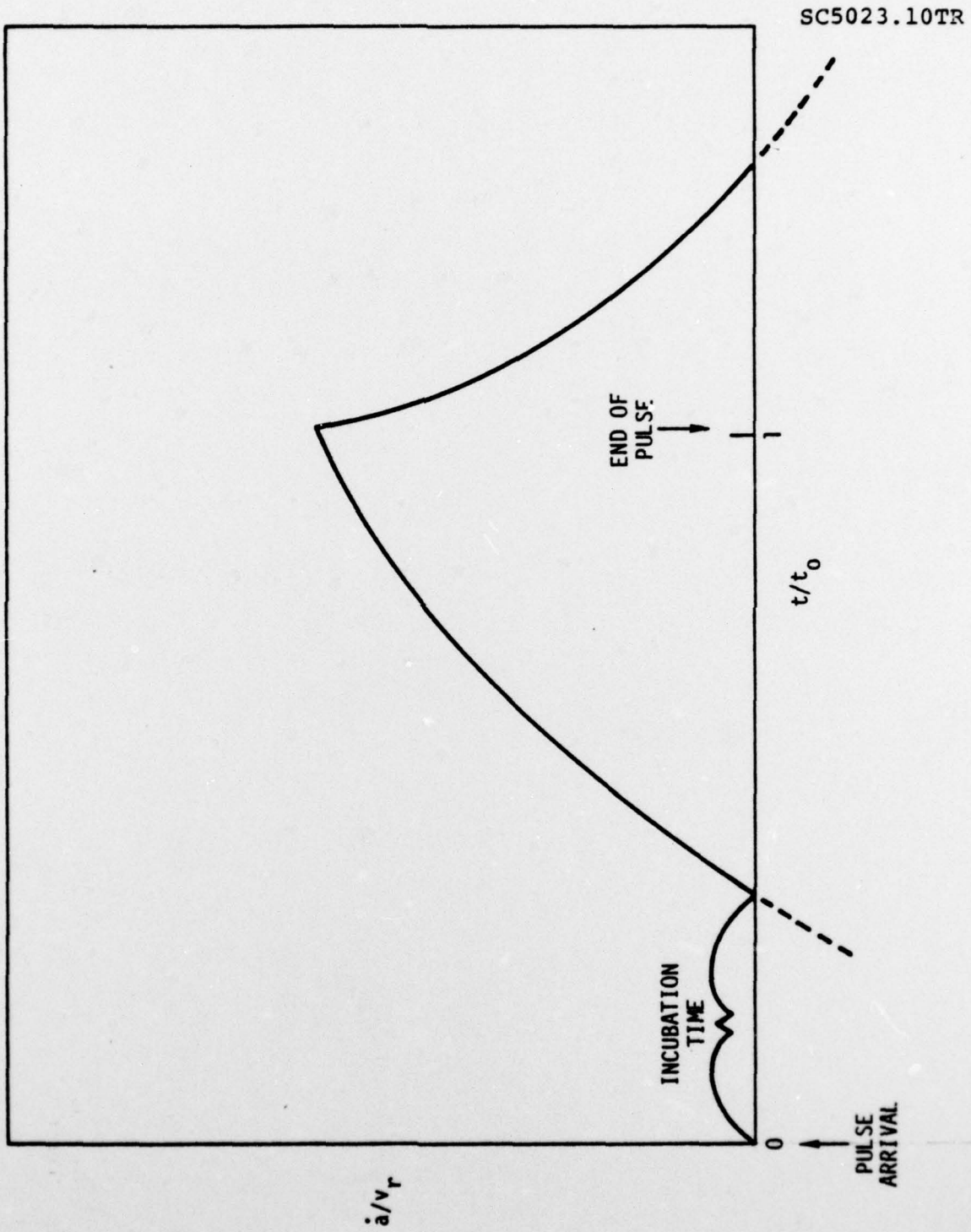
SC5023.10TR
END OF PULSE
1
t/t_o
INCUBATION TIME
0
PULSE ARRIVAL
$\dot{a}/v_r$

Figure 7

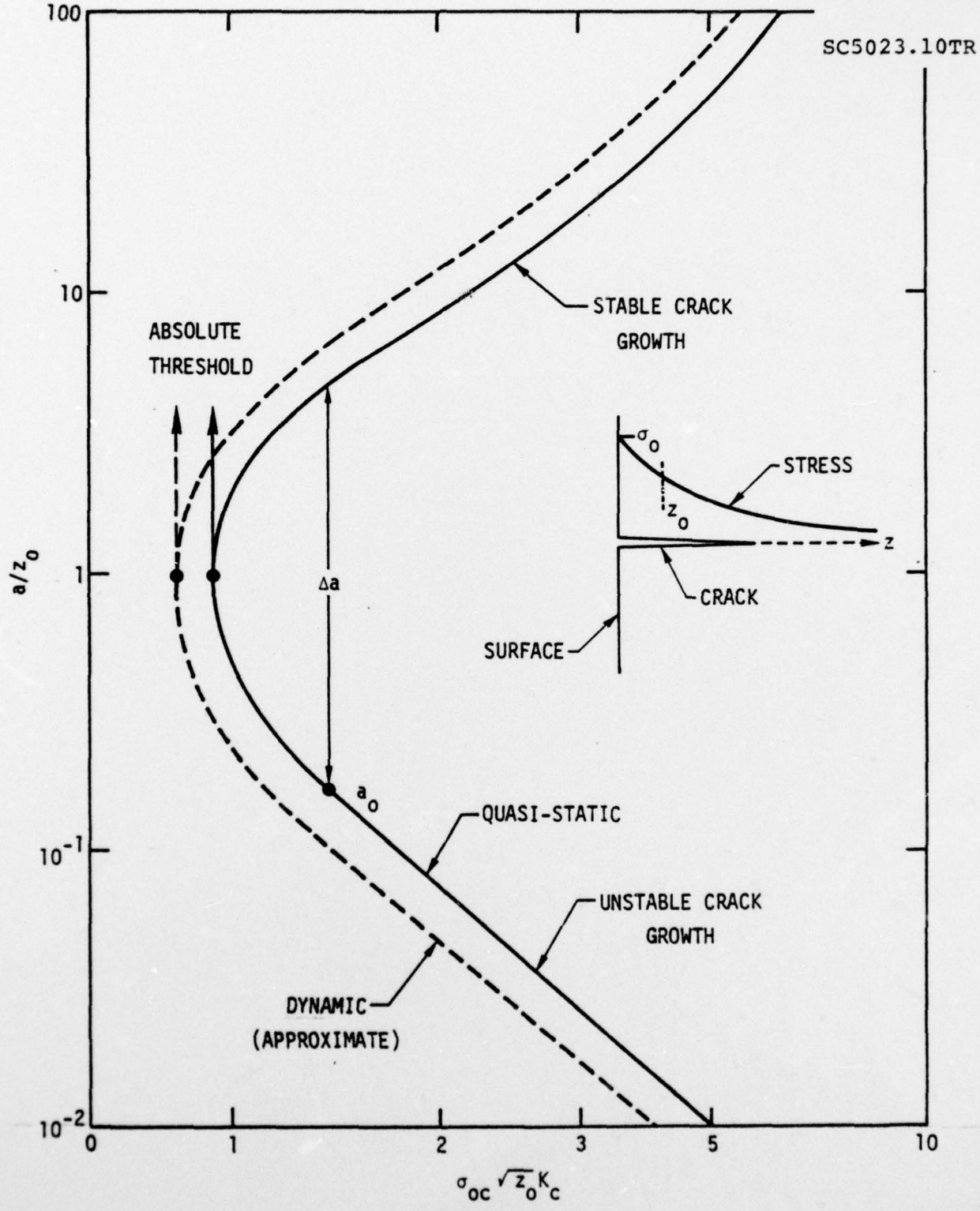
SC5023.10TR
100
10
1
10^{-1}
10^{-2}
a/z_o
0
1
2
3
5
10
$\sigma_{oc}\sqrt{z_o}K_c$
STABLE CRACK GROWTH
ABSOLUTE THRESHOLD
Δa
a_o
QUASI-STATIC
UNSTABLE CRACK GROWTH
DYNAMIC (APPROXIMATE)
σ_o
STRESS
z_o
z
CRACK
SURFACE

Figure 8

Figure 9